Adhesive and healable supramolecular comb-polymers

Reactive and Functional Polymers 202 (2024) 105994

Contents lists available at ScienceDirect

Reactive and Functional Polymers

journal homepage: www.elsevier.com/locate/react

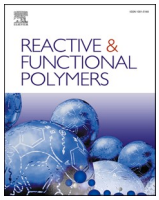

Adhesive and healable supramolecular comb-polymers

Zhenping Shi [a], Matthew Hyder [a], Alarqam Z. Tareq [a], Ann M. Chippindale [a], James A. Cooper [a], Josephine L. Harries [b], Wayne Hayes [a,*]

[a] Department of Chemistry, University of Reading, Whiteknights, Reading RG6 6DX, UK
[b] Domino UK Ltd, Trafalgar Way, Bar Hill, Cambridge CB23 8TU, UK

ARTICLE INFO

Keywords:
Supramolecular material
Adhesive
Healable
Amide recognition units
Comb-polymer

ABSTRACT

A series of supramolecular comb polymers (SCPs) with adhesive and healable characteristics have been generated through the copolymerisation of methacrylate monomers featuring aromatic amide functionalities with lauryl methacrylate. By varying the amide functionality and loading of the supramolecular monomers, the properties of the resulting SCPs can be tailored, ultimately providing stable films at room temperature. As the loading of the amide-bearing monomer was increased, the phase separation between the hard and soft domains was enhanced, promoting larger hard-domain aggregation, as observed via atomic force microscopy (AFM). The mechanical properties of the SCPs correlated to the loading of the amide-bearing monomers, by increasing the mol% incorporation the resulting SCPs transition from possessing high strain to high ultimate tensile strength (UTS) and Young's modulus (YM). Over several re-adhesion cycles, the SCPs were shown to retain their shear strength when thermally adhered to both glass and aluminium substrates. Additionally, the SCPs exhibited healable properties at elevated temperatures (> 45 °C) allowing for the recovery of mechanical properties post-damage.

1. Introduction

Supramolecular polymers have garnered significant interest arising from the dynamic and highly directional nature of the non-covalent bonds that create them, affording materials suitable for application in a wide range of fields including, but not limited to, drug delivery, coatings, adhesives, additive manufacturing, sensors, shape memory, and healable coatings [1,2]. The focus on supramolecular polymers derives from their stimuli responsive nature, which is not typically observed with conventional covalently-bonded polymer materials. The incorporation of molecular recognition motifs into macromolecular structures to facilitate generation of dynamic supramolecular networks has been achieved successfully via functionalisation within the polymer main chains [3,4], at polymer chain ends [5–7], and incorporation of pendant groups on comb/brush architectures [8–11]. The marriage between macromolecular structure and mode of supramolecular assembly provides a route to tailor the properties of polymers for specific applications. Widely deployed modes of supramolecular assembly include hydrogen bonding [12–16], π-π stacking [17–19], metal-ligand interactions [6,20,21], and host-guest interactions [22,23].

The use of comb/brush type architectures within supramolecular polymers allows for the generation of large numbers of interchain interactions relative to their telechelic counterparts, enabling enhancement of physical and mechanical properties [24]. Long and co-workers have investigated several hydrogen bonding functionalities as the pendant side units, including nucleobases [25–27], and 2-ureido-4[1*H*]-pyrimidone (UPy) [11,28]. Through the copolymerisation of butyl acrylate with a UPy functionalised methacrylate monomer, a series of supramolecular thermoreversible comb polymers have been realised [11]. This study revealed a threefold increase in the peel strength from glass with incorporation of only 3.3 mol% of the UPy monomer, when compared to homo poly(butyl acrylate).

The ability of supramolecular polymer networks to recover their physical properties post-damage has been widely investigated with use of different assembly groups, macromolecular structures, and external stimuli to induce healing. Hydrogen bonding units have been employed successfully as the reversible non-covalent component within healable polymer networks. For example, Weder and co-workers [29] utilised the UPy functional unit to form trifunctional, low molecular weight monomers, which form a supramolecular polymer glass with the ability to

* Corresponding author.
E-mail addresses: zhenping.shi@pgr.reading.ac.uk (Z. Shi), m.hyder@pgr.reading.ac.uk (M. Hyder), a.z.tareq@pgr.reading.ac.uk (A.Z. Tareq), a.m.chippindale@reading.ac.uk (A.M. Chippindale), james.cooper@reading.ac.uk (J.A. Cooper), josie.harries@domino-uk.com (J.L. Harries), w.c.hayes@reading.ac.uk (W. Hayes).

https://doi.org/10.1016/j.reactfunctpolym.2024.105994
Received 23 April 2024; Received in revised form 12 June 2024; Accepted 21 June 2024
Available online 22 June 2024

rapidly heal in the presence of UV light. A supramolecular polyurethane capable of healing at body temperature was developed by Feula et al. [15]. The end-capped telechelic system exhibited complete recovery of the mechanical properties within 60 min at 37 °C and retained its self-healing characteristics when to adhered to porcine skin. Supramolecular brush-polymers developed by Guan and co-workers [30] utilised polyacrylate amide side chains on a polystyrene backbone to realise self-healing thermoplastic elastomers. These supramolecular brush-polymers were shown to be capable of spontaneous self-healing at room temperature with up to 92% recovery of extensibility after 24 h.

The amide functional group provides directional hydrogen bonding interactions and has been incorporated in a diverse range of polymer types including dendrons, proteins, and supramolecular assemblies [31,32]. Notable examples of polyamides include Nylon and Kevlar, which exhibit impressive mechanical properties on account of the highly directional and strong hydrogen bonding between amide motifs [33]. Self-complementary benzene-1,3,5-tricaboxamides form well-defined aggregates, both in the solid state and in solution, via association of amide units [34,35], enabling the generation of microcapsules [36], organogelators [37], liquid crystals [38], and nanostructured materials [39,40]. We have recently investigated aliphatic amide functionality of end-caps on telechelic polyurethanes [41]. In comparison to related supramolecular polyurethane systems, the enhanced association between polymer chains featuring these end groups resulted in significant increases in the Young's modulus (YM) and ultimate tensile strength (UTS) from the addition of just two aliphatic amide groups to the polymer end-cap.

This paper reports the design, synthesis and property assessment of a series of supramolecular *comb*-polymers (SCPs) based upon a methacrylate backbone that features variable loadings of aromatic amide side chain units which promote self-assembly via hydrogen bonding interactions. The introduction of novel supramolecular monomers with lauryl methacrylate produces thermally stable films at room temperature with both adhesive and healable properties. Additionally, this study explores the key role of amide functionality in reinforcing the thermal, rheological, and mechanical properties of supramolecular comb polymers.

2. Experimental

2.1. Materials

4-Nitrophenol was purchased from Tokyo Chemical Industry Co. Ltd., palladium on carbon 10 wt% and AIBN were purchased from Sigma Aldrich, 4-aminobenzoic acid was purchased from Alfa Aesar. All other reagents used were purchased from Sigma Aldrich, TCI, Acros Organics, Fisher Chemical, and Fluorochem and used as received. THF, DMF, and dichloromethane were dried prior to use using an MBRAUN SP7 system fitted with activated alumina columns. All other chemicals were used without further purification. 1-Nitro-4-(octyloxy) benzene, 4-(octyloxy) aniline and 4-((*tert*-butoxycarbonyl)amino)benzoic acid were synthesized using modifications of reported procedures [42–44] – the synthesis and analysis of these compounds, together with **1**–**6** and the polymers poly(lauryl methacrylate) (**PLMA**) and **SCP1**–**10** is reported in the Supporting Information (SI) file (see **Table S1** for the monomer feed ratios used).

2.2. Characterization

^{1}H NMR and ^{13}C NMR spectra were recorded on either a Bruker Nanobay 400 or a Bruker DPX 400 spectrometer operating at 400 MHz for ^{1}H NMR or 100 MHz for ^{13}C NMR spectroscopic analysis. Samples for NMR spectroscopic analysis were prepared in $CDCl_3$, DMSO-d_6, with dissolution aided by gentle heating if necessary. Infrared (IR) spectroscopic analysis was carried out using a Perkin Elmer 100 FT-IR (Fourier Transform Infrared) instrument with a diamond-ATR sampling accessory. Mass spectrometry (MS) was conducted using a ThermoFisher Scientific Orbitrap XL LCMS. The sample was introduced by liquid chromatography (LC), and sample ionization was achieved by electrospray ionization (ESI). Melting points were recorded using a Stuart MP10 melting point apparatus and are uncorrected. An Agilent Technologies 1260 Infinity system was used to obtain gel permeation chromatography (GPC) analysis in HPLC-grade THF at a flow rate of 1.0 mL min^{-1}. Calibration was achieved using a series of near monodisperse polystyrene standards, and samples were prepared at a concentration of 1.0 mg mL^{-1}. Differential calorimetry (DSC) measurements were performed on a TA Instruments DSC Q2000 adapted with a TA Refrigerated Cooling System 90, using aluminium TA Tzero pans and lids, measuring from −80 °C to 180 °C with a heating and cooling rate of 5 °C min^{-1}. Thermogravimetric analysis (TGA) was carried out on TA Instruments TGA Q50 instrument with aluminium TA Tzero pans. The sample was heated from 20 °C to 550 °C at 10 °C min^{-1} under nitrogen gas with a flow rate of 100 mL min^{-1}. Rheological measurements were performed on a Malvern Panalytical Kinexus Lab+ instrument fitted with a Peltier plate cartridge and 8 mm parallel plate geometry. Tensile tests were carried out using a Thümler Z3-X1200 tensometer at a rate of 10 mm min^{-1} with a 1 KN load cell. The modulus of toughness was calculated by integrating the recorded plot to give the area under the curve. The trapezium rule was applied to calculate the area between zero strain to strain at break for each sample. The Young's modulus was determined to be the gradient of the linear region of the stress-strain curve passing through the origin and the ultimate tensile strength was recorded as the highest strain value for each curve. The error reported is the standard deviation for the three repeats for each sample. A Mettler–Toledo hot-stage microscope was employed to study the healing characteristics of the comb polymers. The polymers were placed on glass slides and heated at a rate of 2 °C min^{-1} from 25 °C to 150 °C and recorded at 1 fps.

The atomic force microscopy (AFM) was conducted in the Centre for Advance Microscopy (CfAM) at the University of Reading using the Cypher S AFM (Oxford Instruments-Asylum Research, Santa Barbara, USA). The AFM stage movement within the *x*, *y* and *z* directions was controlled using piezoelectric stacks. The scans were recorded through the user interface, Igor Pro (Version 16.33.234), using the standard Alternating Contact (AC) Topography mode (tapping mode) operating in air using a silicon tip with a resonant frequency set at approximately 70 kHz and a spring constant of approximately 2.0 Nm^{-1} (AC240TS-R3, Oxford Instruments). Each sample (0.5 mg mL^{-1} in DMF) was drop cast onto a 10 mm diameter AFM mica disc, first cleaved with Sellotape. Each disc was mounted onto 15 mm diameter magnetic stainless steel AFM specimen discs using 9 mm diameter carbon adhesive tabs and secured onto the microscope scanner stage magnetically. Then, through the user interface, the objective focus was adjusted and set to focus on the tip and on each sample in turn. The cantilever was autotuned at its resonant frequency which automatically determined the drive amplitude and drive frequency. The resolution, scan rate, integral gain and scan size were entered into the user interface before starting the scan. The software Gwyddion (version 2.63) was used for data analysis and editing.

A crystal of **5** was mounted under Paratone-N oil and flash cooled to 100 K under nitrogen in an Oxford Cryosystems Cryostream. Single-crystal X-ray intensity data were collected using a Rigaku XtaLAB Synergy diffractometer (Cu Kα radiation (λ = 1.54184 Å)). The data were reduced within the CrysAlisPro software [45]. The structures were solved using the program Superflip [46] and all non-hydrogen atoms were located. Least-squares refinement against F was carried out using the CRYSTALS suite of programs [47]. The non-hydrogen atoms were refined anisotropically. All the hydrogen atoms were located in difference Fourier maps The hydrogen atoms were placed geometrically with a C—H distance of 0.95 Å, an N—H distance of 0.85 Å and a U_{iso} of ~1.2–1.5 times the value of U_{eq} of the parent atom, and the positions refined with riding constraints. The carbon atoms C30-C36 in the octane tail were modelled as disordered over two sites.

3. Results and discussion

3.1. Monomer synthesis

The focus of this study was the incorporation of aromatic amide side-chain units in a *comb*-polymer architecture to promote interchain assembly and network formation via hydrogen bonding. The synthesis began with the coupling of 4-nitrophenol with 1-bromooctane under Williamson ether type conditions to generate 1-nitro-4-(octyloxy)benzene that was then reduced in 91% yield using hydrogen over palladium on carbon to the corresponding aniline (Scheme 1). 4-(Octyloxy) aniline was then coupled with 4-((*tert*-butoxycarbonyl)amino)benzoic acid using EDC·HCl and DMAP to afford the protected aromatic amide **1**. Treatment of **1** with TFA gave the corresponding aniline **2**, which was then deployed in two pathways (see Scheme 1). To increase the number of hydrogen bonding groups, aniline **2** was coupled with 4-((*tert*-butoxycarbonyl)amino)benzoic acid to afford the protected bisamide **3**. Exposure of **3** to TFA yielded the desired bisamide-aniline **4**. The anilines **2** and **4** were then coupled independently to 2-isocyanatoethyl methacrylate to afford the desired methacrylate monomers **5** and **6** capable of hydrogen bonding via aromatic amide units. The synthetic procedures used to generate the compounds described above and the associated characterization data (**Figs. S1-S65** and **Tables S2-S4**) are reported in the SI file. The solid-state data for compound **5** is reported in the SI file, see Figs. **S57** and **S58** plus **Tables S2-S4**).

3.2. Polymer synthesis

The supramolecular *comb*-polymers were synthesized via free-radical polymerization utilizing aromatic amide monomers **5** or **6** and lauryl methacrylate (LMA) with AIBN as the radical initiator (Scheme 2). The feed ratios of monomers **5** and **6** were varied between 1 and 15% to generate a series of ten polymers (**SCP1**–**10**) to establish the effect of the aromatic amide side-chain units on the polymer properties relative to **PLMA**. The feed ratio for each material was calculated based on its molar percentage (see **Table S1** in the SI).

Random copolymers **SCP1**–**10** and **PLMA** were generated successfully and characterized by a combination of NMR and IR spectroscopies plus GPC analysis (see Table 1 and the SI **Figs. S66-S112** for the spectroscopic and chromatographic data). As the loading of the aromatic amide monomers **5** or **6** was increased the GPC analysis revealed dramatically increased molecular weights for these materials – probably a consequence of self-association of the polymer chains to yield aggregates under the analytical conditions employed.

3.3. Thermal analysis of *SCP1–10*

The thermal characteristics of the synthesized polymers (**PLMA** and **SCP1**–**10**) were investigated through DSC and TGA analysis, the results are summarised in Table 2. The thermal transitions such as the glass transition (T_g) of these SCPs were probed with sequential heating and cooling cycles in the temperature range of −80 to 200 °C for DSC analysis, with the temperature flow rate of 5 °C min^{-1} for both DSC and TGA.

Through DSC analysis, only glass transitions were observed for **PLMA** and **SCP1**–**10**, revealing the amorphous nature of the polymers and the absence of any long-range ordering within the systems. The homo polymer **PLMA** exhibits a T_g at −54.3 °C, comparable to literature values [48–50]. As the content of monomers **5** or **6** was increased the T_g of the resultant SCP also increased (Fig. 1). This trend was attributed to the increase in intermolecular interactions as a result of the increase in hydrogen bonding functionality of the SCPs. This result is comparable to that reported by Long et al. [11] but differs in that the T_g of their hydrogen bonded *comb*-polymers increased from −50 °C to −23 °C when the feed ratio (mol%) of the UPy-based monomer was increased from 0% to 10%. In direct comparison, the T_g values of **SCP1**–**10** for these systems featuring aromatic amide side-chain units only increase by ca. 15 °C across a similar feed ratio range.

An analogous trend was observed in the TGA studies, in which higher degradation temperatures were observed with higher loadings of the

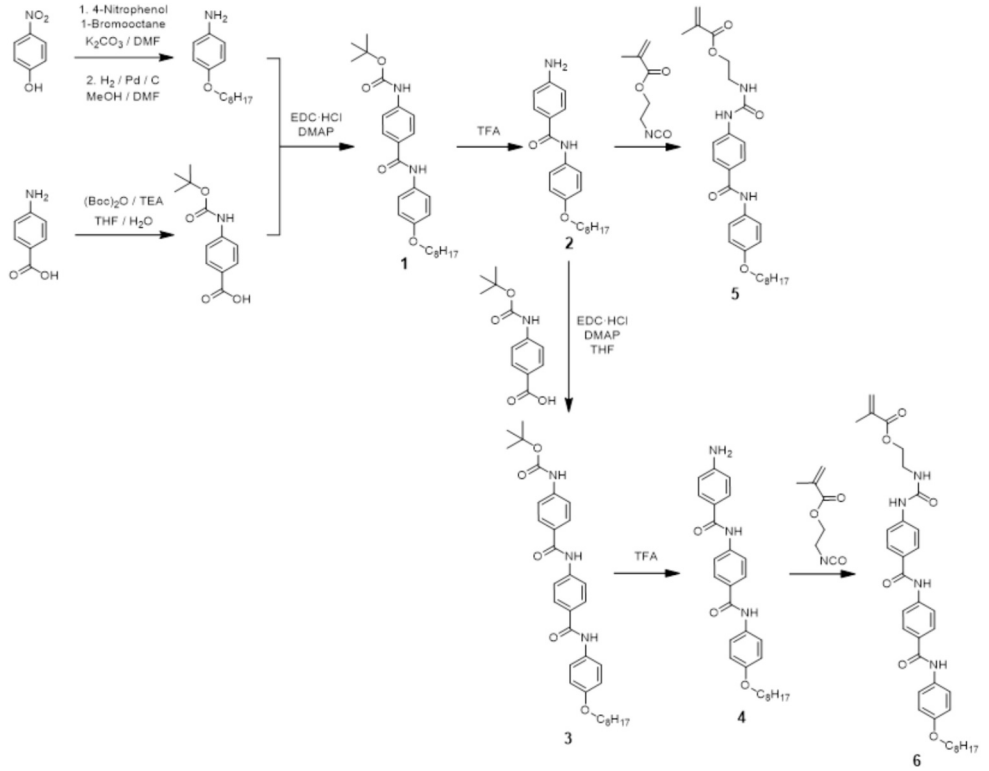

Scheme 1. The synthetic route used to generate the two methacrylate monomers with aromatic amide units (**5** and **6**).

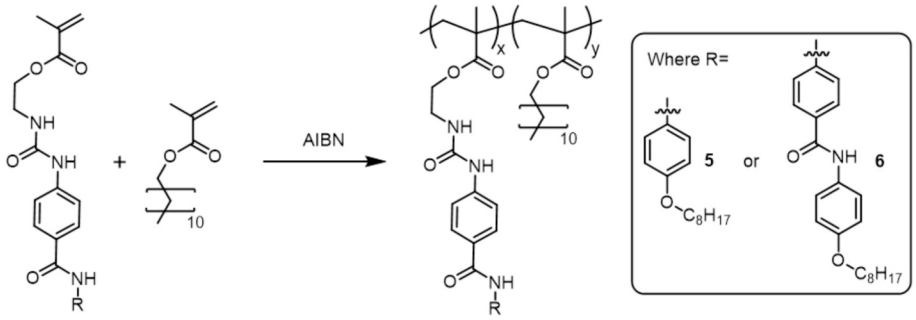

Scheme 2. The structure of the targeted supramolecular *comb*-type polymers.

Table 1
The values of M_n, M_w and Đ of **PLMA** and **SCP1–10**.

Sample	**5** (mol%)	**6** (mol%)	M_n (kg mol^{-1})	M_w (kg mol^{-1})	Đ
PLMA	–	–	48	205	4.3
SCP1	1	–	59	310	5.3
SCP2	2.5	–	126	909	7.2
SCP3	5	–	196	1387	7.1
SCP4	10	–	1546	3410	2.2
SCP5	15	–	3716	7023	1.9
SCP6	–	1	53	299	5.7
SCP7	–	2.5	75	512	6.8
SCP8	–	5	115	1000	8.7
SCP9	–	10	155	1527	9.9
SCP10	–	15	174	1858	10.7

Table 2
The thermal analysis data of **PLMA** and **SCP1–10**.

Sample	T_g (°C)	Onset of degradation (°C)
PLMA	−54.3	244.2
SCP1	−53.6	256.4
SCP2	−50.6	256.2
SCP3	−49.0	256.3
SCP4	−46.2	258.8
SCP5	−40.5	264.0
SCP6	−51.2	253.0
SCP7	−50.6	265.1
SCP8	−47.2	265.2
SCP9	−43.7	261.4
SCP10	−39.3	261.7

supramolecular monomer (see **Fig. S124-S134**). The trend of both thermal analyses shows that the addition of either monomer, **5** or **6**, increases the thermal stability of the polymer. This conclusion can also be drawn from the gradual increase in the slope of the TGA plot (see **Fig. S135** in the SI).

3.4. Atomic force microscopy

The microphase separation between the polymer segments was investigated by atomic force microscopy (AFM), see Fig. 2 and **Figs. S136–138**. The AFM images in Fig. 2 and **Fig. S137** show the phase topography mode of polymer samples at scan size 5 μm and 2 μm, respectively, while **Fig. S136** and **Fig. S138** show AFM height images recorded in topography mode at 5 μm and 2 μm, respectively. AFM analysis of each polymer revealed two distinct phases: the hard segments were evident as dark areas as a result to the low phase angle, and the bright regions were attributed to the soft domains on account of the high phase angle [51].

A few dark areas were observed in **SCP3**, as shown in Fig. 2 (A), corresponding to aggregation of the hard segments via hydrogen bonding and aromatic π–π stacking between polymer chains [52]. The light areas of the images, evident as continuous phases, corresponded to

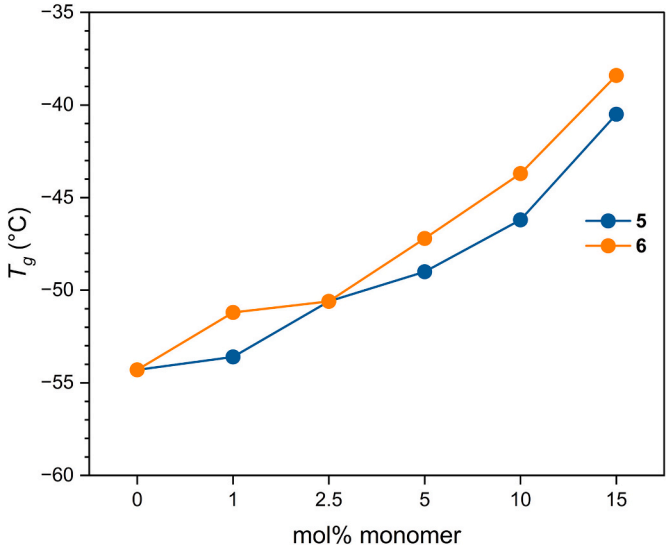

Fig. 1. The relationship between the mol% of monomer **5** or **6** in the supramolecular comb polymers and their T_g values.

the soft segments of the polymers. A higher abundance of well-defined aggregated hard segments was observed in the case of **SCP4**, arising from the strong phase separation resulting from the increase in loading of monomer **5** and the amplification of supramolecular interactions this provides. A drastic increase in phase separation was evident in **SCP5**, when compared to **SCP3** and **SCP4**, and is displayed as aggregated micro-sheets [53] as a result of strong associations between the polymer chains derived from the high mol% of **5** (15 mol% for **SCP5**) which introduces strong and highly directional assembly of the supramolecular functionalities, such as the amide and urea units.

The addition of an additional aromatic amide in **6** (when compared to **5**) gives rise to more well-defined microphase separation in **SCP8–10** in comparison to **SCP3–5**. For example, the images of **SCP9** in Fig. 2 (E) and **Fig. S137** (D) reveal larger assemblies of the dark areas [54], these hard segments become more aggregated and appear as short 'wormlike' aggregates as a result of strong association via the enhanced hydrogen bonding provided by the amide functionalities in **6** when compared to **SCP4** which contains **5**. In **SCP10** the introduction of 15 mol% of **6** produces exceptional microphase separation. Owing to the extremely strong association provided by the enhanced hydrogen bonding of the additional amide within **6**, the large aggregated hard segments were dispersed through the continuous soft segments. In addition, bright 'wormlike' shapes are clearly evident and could be attributed to the agglomeration of polymeric nanoparticles formed from intrachain association [55], these agglomerations are shown to have diameters around ca. 400–500 nm which contain nanoparticles of ca. 40–55 nm, see **Fig. S139A** and **S139B**, respectively. This differs significantly from

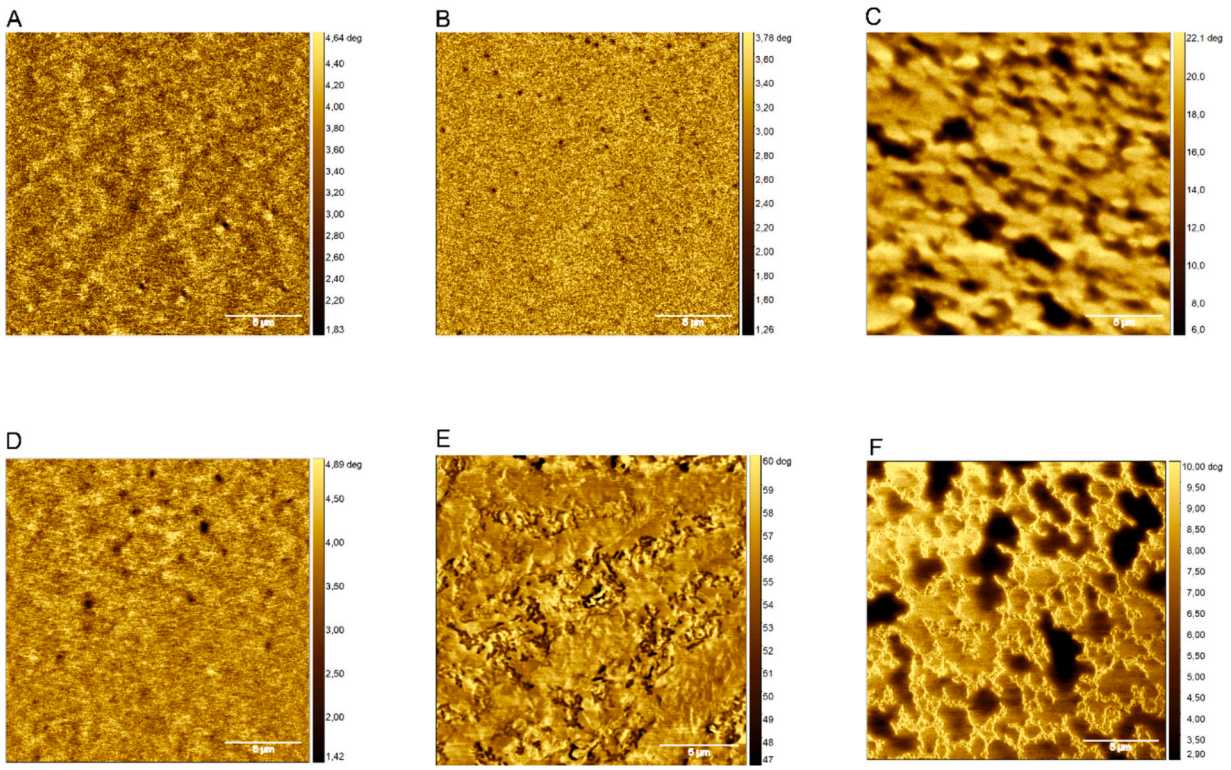

Fig. 2. AFM tapping mode phase images of **SCP3** (A), **SCP4** (B), **SCP5** (C), **SCP8** (D), **SCP9** (E), and **SCP10** (F); the scale bars = 5 μm. All the SCP samples were prepared by drop casting from THF (0.5 mg mL^{-1}) on freshly cleaved mica discs.

the surface morphology of **SCP5**, which shows very flat rounded features with larger surface areas at the same mol% loading.

3.5. Rheological analysis

The viscoelastic properties of **PLMA** and **SCP1**–**10** were assessed with dynamic rheological testing, within a temperature range of 0 °C to 150 °C at a normal force of 1 N and a frequency of 1 Hz. The storage modulus (G') and phase angle (δ) were recorded against temperature according to the monomer used, which were divided into two groups (**5** and **6**, **Fig. 3**(**a**) and **3**(**b**), respectively).

From Fig. 3, it is evident that the storage modulus increases as the monomer feed of the aromatic amide monomers increases, and the significant increase in the energy storage modulus arises from increased hydrogen-bonding interactions in the polymer network. For example, **SCP4** undergoes a viscoelastic transition at ~80 °C when the monomer loading of monomer **5** is 10%. In contrast, in the case of polymer **SCP9** (with the same monomer loading value but incorporating monomer **6** that features two amide units) does not exhibit a viscoelastic transition across the temperature range studied (i.e. up to 150 °C). This observation can be attributed to the hydrogen bonding potential of the different monomer subunits **5** and **6** within the comb polymers. In comparison to SCPs featuring the aromatic amide **5**, SCPs that incorporate monomer **6** must be exposed to higher temperatures to reach the viscoelastic transition at the same molar percentage feed of the aromatic amide monomers.

3.6. Tensile testing

The SCPs were cast from solution to form uniform films, the stability of these films in conjunction with the rheological analysis conducted established that the polymers **SCP4**, **SCP5**, **SCP8**, **SCP9**, and **SCP10** form stable, pliable, and elastic films at room temperature. However, the other polymers (**PLMA**, **SCP1**, **SCP2**, **SCP3**, **SCP6**, and **SCP7**) were found to be viscous liquids and afford unstable films that are unsuitable for tensile testing at ambient temperature. The polymer films were cut into rectangular strips of uniform thickness of 2 cm × 0.5 cm (L × W) and each polymer was tested in triplicate. The tensile data thus obtained for **SCP4**, **SCP5**, **SCP8**, **SCP9**, and **SCP10** are shown in Fig. 4.

The values of the modulus of toughness (MoT), Young's modulus (YM), modulus of resilience (MoR), ultimate tensile strength (UTS), strain at break, and stress at break were then calculated and the average values are detailed in Table 3. Increasing the mol% of the aromatic amide monomers (**5** and **6**) in the SCPs significantly increases the YM and UTS whilst significantly decreasing the strain at break; a trend also observed by Wu et al. [56] with their UPy functionalisation of poly (glycerol sebacate). Increasing the incorporation of monomer **5** from 10 mol% (**SCP4**) to 15 mol% (**SCP5**) affords a dramatic enhancement of the YM, from 1.08 ± 0.1 MPa to 23.74 ± 2.1 MPa, and a concomitant decrease in the strain at break, from 13.29 ± 1.2 ε to 0.33 ± 0.03 ε. Incorporating monomer **6** increases the number of amide units, giving SCPs that exhibit lower UTS, YM, and strain at break when compared to SCPs containing monomer **5** at comparable loadings. For example, with 15 mol% monomer loading the YM drops from 23.74 ± 2.1 MPa (**SCP5**, monomer **5**) to 2.11 ± 0.3 MPa (**SCP10**, monomer **6**) and with 10 mol% monomer loading the strain at break drops from 13.29 ± 1.2 ε (**SCP4**, monomer **5**) to 2.11 ± 0.3 ε (**SCP9**, monomer **6**). The trends with **SCP8**–**10** containing monomer **6** can potentially be ascribed to increased intrachain association, and subsequent nanoparticulate formation at high mol% loadings [55], as seen in Fig. 2F with **SCP10**. To place these SCPs into context with regard to our previously published telechelic polyurethanes [14–16,41,57,58], **SCP5** outperforms many in terms of YM and UTS, with **SCP4** also possessing enhanced strain at break. In related studies on supramolecular polymer architectures, an ABA block copolymer reported by Guan and co-workers [59], featuring poly (methyl methacrylate) and poly(acrylate amide) blocks, was also shown to outperform their previously published comb [60] and brush [30,61] copolymers both in terms of YM and UTS.

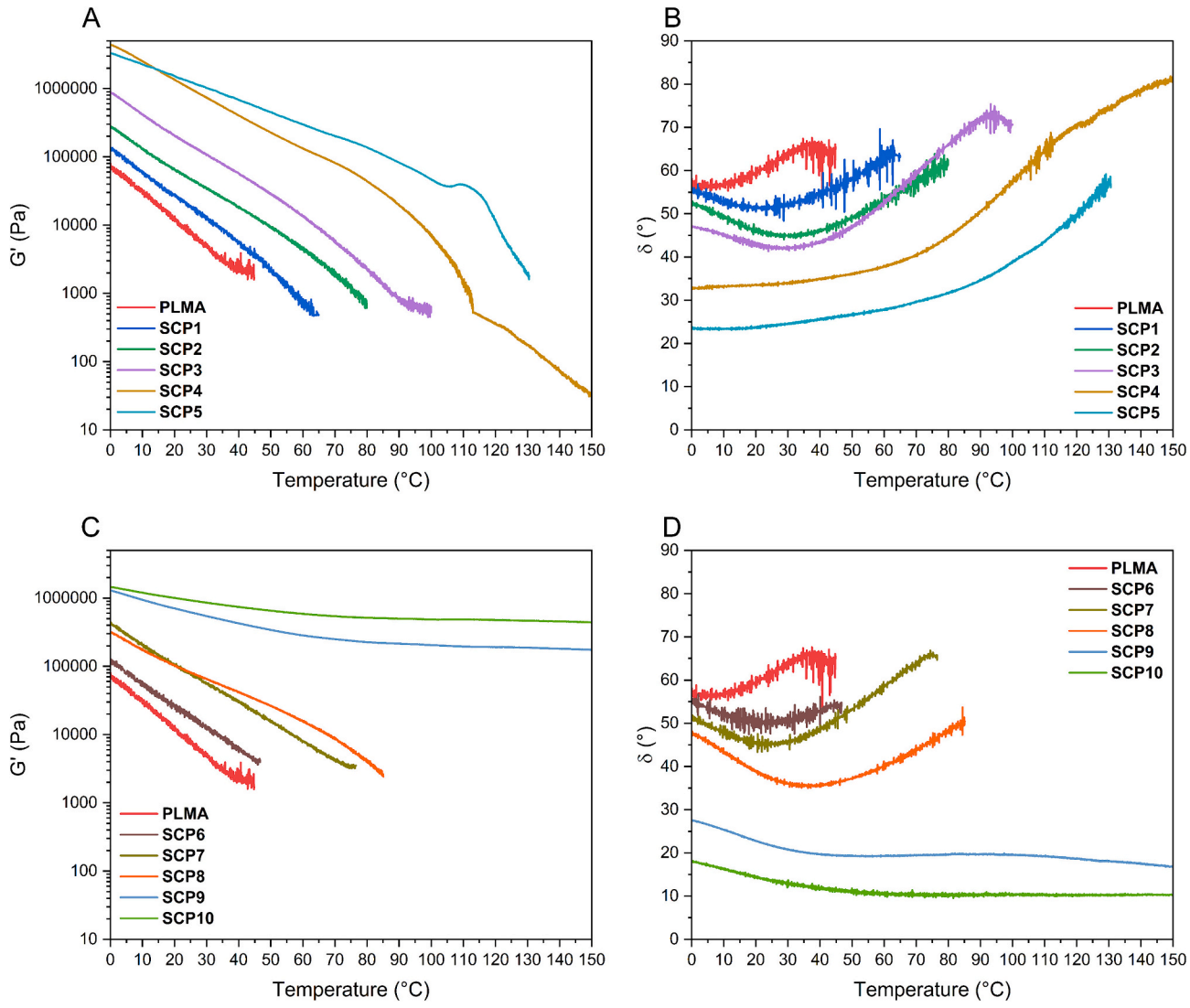

Fig. 3. The plots of G′ (**A**) and δ (**B**) vs. temperature for supramolecular comb polymers **SCP1**–**5** and the plots of G′ (**C**) and δ (**D**) vs. temperature for supramolecular comb polymers **SCP6**–**10**.

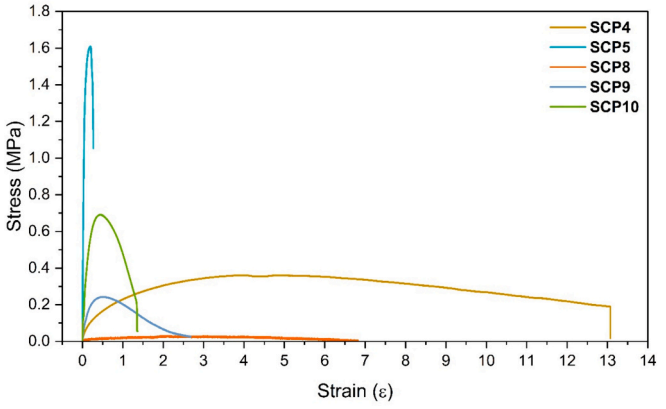

Fig. 4. Representative stress-strain curves of **SCP4**, **SCP5**, **SCP8**, **SCP9**, and **SCP10**.

Table 3
The values of Modulus of Toughness, Young's Modulus, Modulus of Resilience, Ultimate Tensile Strength, Strain at break, Stress at break of **SCP4**, **SCP5**, **SCP8**, **SCP9**, and **SCP10**.

Polymer	Modulus of Toughness (MPa)	Young's Modulus (MPa)	Modulus of Resilience (KPa)	UTS (MPa)	Strain at break (ε)	Stress at break (MPa)
SCP4	4.05 ± 0.20	1.08 ± 0.1	2.36 ± 1.1	0.39 ± 0.01	13.29 ± 1.2	0.22 ± 0.04
SCP5	0.40 ± 0.04	23.74 ± 2.1	42.76 ± 3.2	1.41 ± 0.1	0.33 ± 0.03	0.90 ± 0.07
SCP8	0.10 ± 0.00	0.03 ± 0.01	9.15 ± 1.7	0.03 ± 0.00	5.75 ± 0.5	0.01 ± 0.00
SCP9	0.30 ± 0.03	1.75 ± 0.3	6.17 ± 1.1	0.23 ± 0.02	2.11 ± 0.3	0.02 ± 0.01
SCP10	0.71 ± 0.06	3.65 ± 0.25	65.49 ± 6.2	0.70 ± 0.03	1.36 ± 0.02	0.14 ± 0.03

3.7. Adhesion tests

To investigate the adhesive capabilities of the SCP polymers, samples of uniform thickness were cut into 0.5 cm × 0.5 cm squares, sandwiched between silica glass slides or aluminium sheets and then held with a clamp to ensure contact between the polymer film and substrate sheets. After being placed in an oven for 2 h (that was held at ca. 10 °C below the viscoelastic transition of the polymer i.e. **SCP9** and **SCP10** were adhered at 110 °C and 120 °C, respectively), the polymer films were left at room temperature for half an hour to cool before being subjected to simple tensile experiments. Each polymer was analysed in triplicate (see Fig. 5 and Table 4). The sample with the highest tensile force was selected and the experiment was then repeated three further times to investigate the re-adhesive capability of the samples.

For both glass and aluminium, increasing the mol% of the functional monomer (**5** or **6**) results in an increase in the shear strength. For example, with a 10 mol% increase in monomer **6** the shear strength on aluminium increases by 424%, from 0.25 ± 0.01 MPa (**SCP8**) to 1.06 ± 0.04 MPa (**SCP10**). The poor adhesion to glass and aluminium surfaces of **SCP8**–**10** can be attributed to the increase in amide functionality of monomer **6**. This increases the crosslink strength and density, ultimately hindering thermal dissociation of the supramolecular interactions during the adhesion process, a similar phenomenon was observed by Tareq et al. [41] with their amide functionalised telechelic polyurethanes. As a result, a minimum decrease in shear strength of ca. 50% is observed for **SCP9** and **SCP10** for both glass and aluminium when compared to **SCP4** and **SCP5**, which possess comparable monomer loadings. Therefore, **SCP5** possesses the highest shear strength of 2.10 ± 0.08 MPa and 2.90 ± 0.1 MPa on glass and aluminium, respectively. To put this data into context, our best adhesive on glass, **SCP5**, exhibits an increase in shear strength of 75% and 1650%, respectively, when compared to isophthalic acid-functionalized soybean oil [62] and statistical comb copolymer blends featuring complementary nucleobase functionality (adenine and thymine) [26].

From the short series of SCPs tested, **SCP5** outperformed the other SCPs in terms of shear strength on both glass and aluminium substrates. This performance, in conjunction with its low adhesive temperature of 100 °C, meant it was an excellent candidate for the investigation of the re-adhesive capabilities of SCPs of this type. The shear strength was investigated in triplicate over three re-adhesion cycles and the results are reported in Fig. 6 and Table 5.

After three re-adhesion cycles, **SCP5** retained its shear strength when adhered to glass (from 2.10 ± 0.1 MPa to 2.18 ± 0.1 MPa) and aluminium over the three re-adhesion cycles (from 2.90 ± 0.1 MPa to 3.17 ± 0.15 MPa), see Fig. 6. This phenomenon of shear strength retention is characteristic of supramolecular adhesives that undergo dynamic assembly, for example, Feringa, Tian, and *co*-workers observed maintenance of shear strength over 30 re-adhesion cycles for their poly (thioctic acid) copolymer [63].

To further investigate the adhesive stability of **SCP5**, two lap shear samples were prepared using the same method employed for the adhesion tests and then a 2 lb. (0.907 Kg) weight was suspended from the base of the sample 24 h. No deformation was observed across this timeframe, see **Fig. S155**.

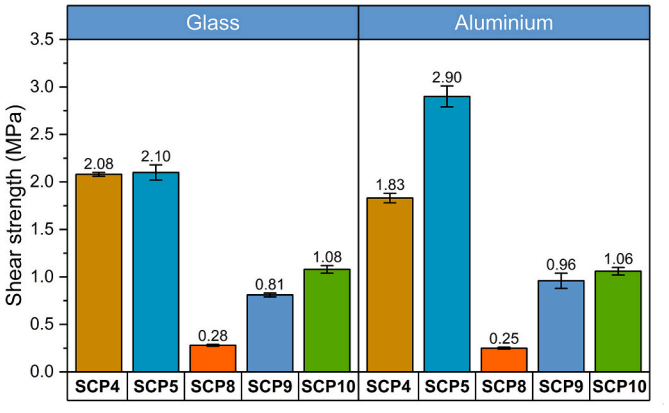

Fig. 5. Plots of the shear strength of the SCPs in relation to the mol% content of the aromatic amide monomers.

Table 4
Shear strength for comb polymers **SCP4**, **SCP5**, **SCP8**, **SCP9**, and **SCP10** on glass sheet and aluminium sheet.

Samples	Shear strength (MPa) glass	Shear strength (MPa) aluminium
SCP4	2.08 ± 0.02	1.83 ± 0.05
SCP5	2.10 ± 0.1	2.90 ± 0.1
SCP8	0.28 ± 0.01	0.25 ± 0.01
SCP9	0.81 ± 0.02	0.96 ± 0.1
SCP10	1.08 ± 0.04	1.06 ± 0.04

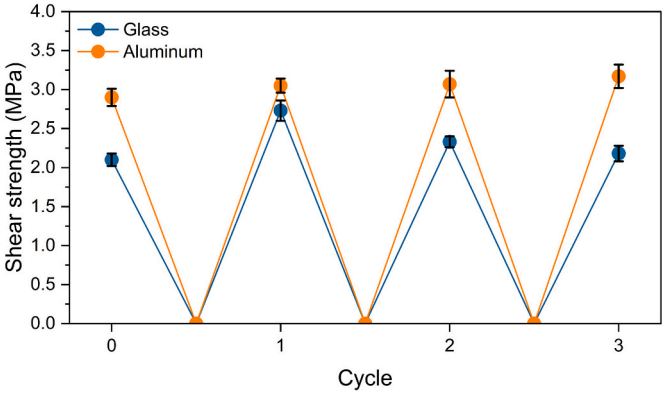

Fig. 6. Shear strength of **SCP5** during three cycles of re-adhesion testing.

Table 5
Adhesion testing of **SCP5** (the data is the average of three repeats).

Number of cycles	shear strength (MPa) glass	shear strength (MPa) aluminium
0	2.10 ± 0.1	2.90 ± 0.1
1	2.73 ± 0.1	3.05 ± 0.1
2	2.33 ± 0.1	3.07 ± 0.2
3	2.18 ± 0.1	3.17 ± 0.15

3.8. Assessment of healing capability

Hot stage microscopic analysis was carried out to monitor the healing process of the SCPs. A sample of uniform thickness (ca. 1 mm) was mounted on a glass slide and then cut in half with a scalpel blade, the two resulting pieces were then placed in close contact, and the slide was placed in the heating chamber. The damaged specimen was then heated from 25 °C at a rate of 2 °C min^{-1}. Pictures of the healing process were taken at four time points: (i) when heating started, (ii) when healing started, (iii) when healing was in progress, (iv) and when healing was complete and heating stopped, and the final temperature recorded. The healing process and temperature of **SCP4**, **SCP5**, **SCP9**, and **SCP10** are shown in Fig. 7.

Increasing the non-covalent crosslink density of the polymer chains through higher incorporation of monomers **5** or **6** within the SCPs shifts the temperature required for the onset and completion of healing to higher temperatures. The addition of the second amide functionality in monomer **6**, compared to monomer **5**, also shifts the healing to higher temperatures, likely due to the higher number of hydrogen bonds. Notably, the absence of a viscoelastic transition of **SCP9** and **SCP10** did

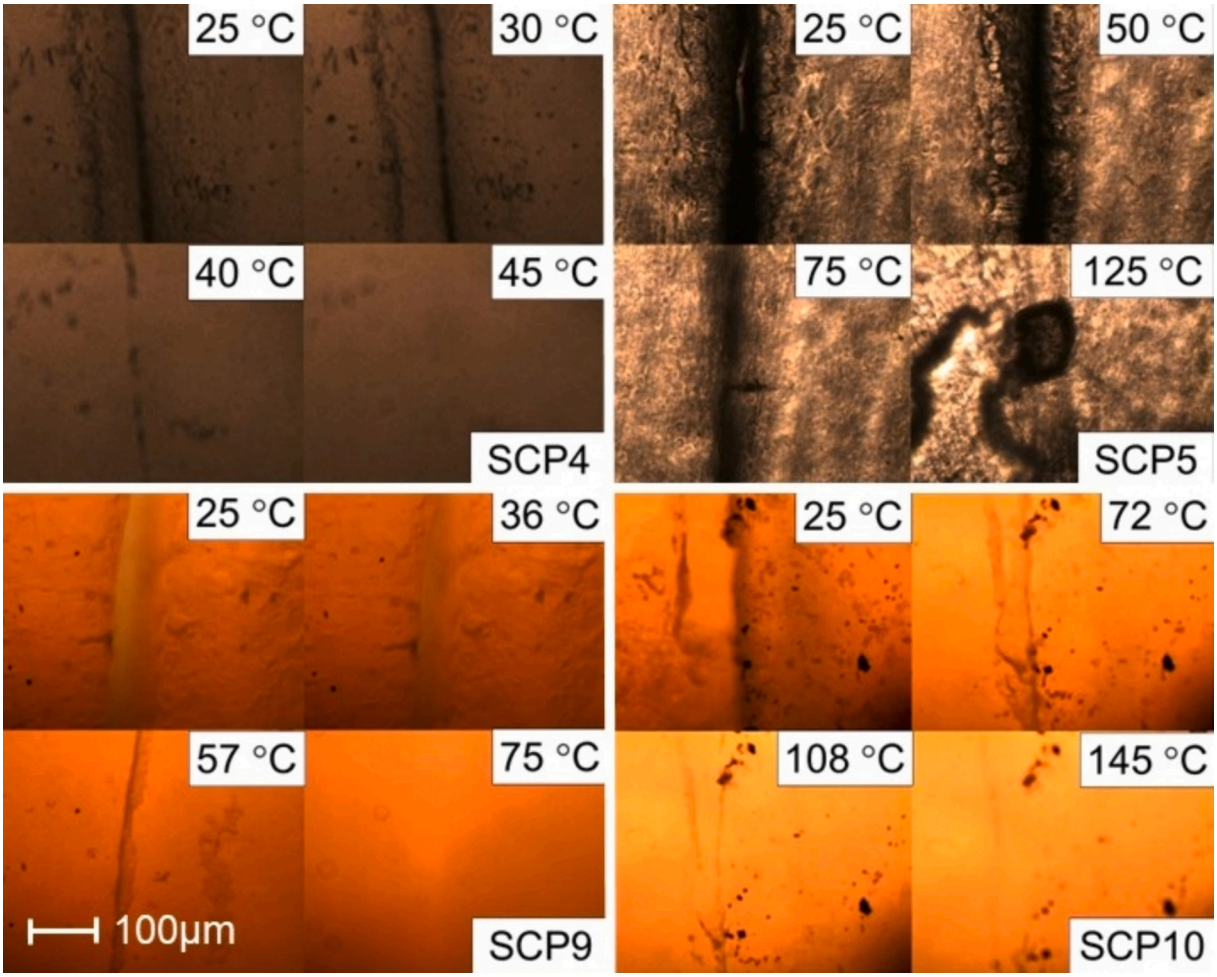

Fig. 7. Hot stage microscope healing tests of **SCP4** (four pictures in the upper left corner); **SCP5** (four pictures in the upper right corner); **SCP9** (four pictures in the lower left corner) and **SCP10** (four pictures in the lower right corner).

not hinder their ability to undergo healing.

In order to examine the recovery of the mechanical properties after healing, the polymer films were cut into rectangular strips of uniform thickness and size (2.0 cm × 0.5 cm, L × W) and cut in half with a scalpel blade [14]. The two pieces were placed in close contact and exposed to a temperature that was held below viscoelastic transition of the polymer by ca. 10 °C for 2 h, followed by a period of 30 min when they were allowed to cool to the ambient temperature of the laboratory. The lower temperature viscoelastic transitions of **SCP4**, **SCP5**, and **SCP8** enabled the polymer samples to heal into a complete film. **SCP9** and **SCP10** required elevated temperatures (>120 °C) to activate the healing process in order to form stable healed regions but at the cost of sample deformation, so these samples were not considered for mechanical assessment. **Fig. S156** shows how the polymer films post-damage and post-healing were inspected prior to assessment via tensile testing.

The healed polymer samples were then subjected to simple tensile experiments and each polymer analysed in triplicate. Representative stress–strain curves of both pristine and healed samples obtained for **SCP4**, **SCP5**, and **SCP8** are shown in Fig. 8 (also see **Figs. S157-S159** in the SI file) with mechanical properties reported in Table 6. Comparison between the pristine and healed samples reveals that **SCP8** exhibits the best healing efficiency of the SCPs tested. **SCP5** exhibits the lowest healing efficiency in terms of MoT and strain at break, 40% and 36%, respectively, resulting from the increased crosslink density provided by the higher mol% of monomer **5** when compared to **SCP4** which observes healing efficiencies of 77% and 74% for MoT and strain at break, respectively. To place this work into perspective, supramolecular brush-

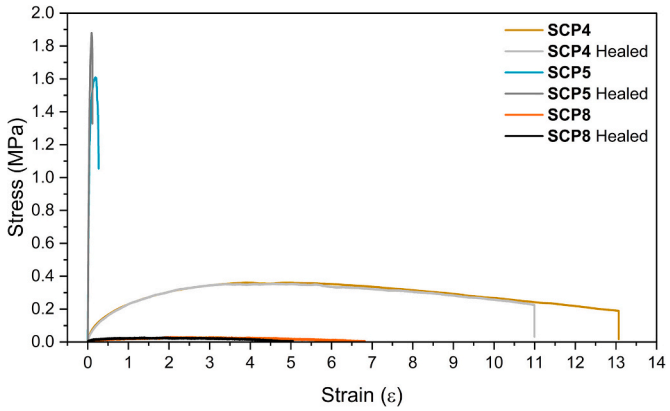

Fig. 8. Representative stress-strain curves of pristine and healed **SCP4**, **SCP5**, and **SCP8**.

polymers generated by Guan and co-workers [30] exhibited almost quantitative recovery of YM after only 15 min of healing at room temperature, however, 24 h was required to obtain 92% recovery of the strain at break. Wang et al. reported [64] the use of isophorone diamine as hard segments in a polyurethane–urea supramolecular composite (PPGTD-IDA) that required 48 h at room temperature to obtain full recovery of the mechanical properties.

Table 6
The tensile data of the pristine (top), healed (middle), and healing efficiency (bottom in bold) for **SCP4**, **SCP5**, and **SCP8.**

Polymer	Modulus of Toughness (MPa)	Youngs Modulus (MPa)	Modulus of Resilience (KPa)	UTS (MPa)	Strain at break (ε)	Stress at break (MPa)
SCP4	4.05 ± 0.2	1.08 ± 0.1	2.36 ± 1.1	0.39 ± 0.01	13.29 ± 1.2	0.22 ± 0.04
	3.13 ± 0.25	1.08 ± 0.15	1.95 ± 0.8	0.39 ± 0.02	9.87 ± 1.25	0.28 ± 0.05
	77%	**100%**	**83%**	**100%**	**74%**	**127%**
SCP5	0.40 ± 0.04	23.74 ± 2.1	42.76 ± 3.2	1.41 ± 0.1	0.33 ± 0.03	0.90 ± 0.1
	0.16 ± 0.01	24.99 ± 2.1	119.16 ± 15.5	1.92 ± 0.1	0.12 ± 0.01	1.42 ± 0.2
	40%	**105%**	**279%**	**136%**	**36%**	**158%**
SCP8	0.10 ± 0.00	0.03 ± 0.01	9.15 ± 1.7	0.03 ± 0.00	5.75 ± 0.5	0.01 ± 0.00
	0.11 ± 0.01	0.08± 0.01	3.11 ± 0.5	0.03 ± 0.00	5.96 ± 0.7	0.01± 0.00
	110%	**267%**	**34%**	**100%**	**104%**	**100%**

4. Conclusions

Two novel aromatic amide monomers **5** and **6,** with varying number of amide functionalities, have been designed, synthesized and fully characterized by NMR and IR spectroscopy together with mass spectrometry. Supramolecular comb-type polymers featuring different loadings of the novel monomers with lauryl methacrylate were generated successfully using a free radical polymerization approach. NMR and IR spectroscopic analysis indicated that the composition of the copolymer was in excellent agreement with the feed ratio used. Consequently, the polymers possessing higher loadings of the aromatic amide monomers **5** or **6** could generate non-covalent crosslinks between chains as a consequence of hydrogen bonding and π–π stacking interactions. Thermal analysis showed that the increase in the aromatic amide monomer loading slightly increased the T_g of the polymer. Rheological analysis and tensile experiments demonstrated that the increase of the aromatic amide monomer content improved the mechanical properties of the polymer. However, too high a loading ultimately renders the polymer brittle in nature, stemming from the increase in phase separation and size of the hard domains, as observed via AFM analysis. Monomer **5** produced SCPs with optimum tensile properties (Young's Modulus = 23.74 ± 2.1 MPa, **SCP5**) and the highest adhesive shear strength (glass = 2.10 ± 0.1 MPa; aluminium = 2.90 ± 0.1 MPa, **SCP5**). Retention of shear strength over three re-adhesion cycles was also achieved with **SCP5** on both glass and aluminium substrates. In addition, five of the comb polymers **SCP4**, **SCP5**, **SCP8**, **SCP9**, and **SCP10,** which are solid at room temperature, exhibited healing capability at elevated temperatures, with **SCP4** exhibiting healing efficiencies of 100% for Young's Modulus and ultimate tensile strength, and 74% for strain at break. Whilst recognising that the the mechanical properties of these SCPs are not directly competitive with commercially available polymers deployed in engineering applications where high modulus is required, modifications to the polymer backbone of these materials via use of higher T_g comonomers or the introduction of additives to form supramolecular polymer blends have been shown to be suitable routes to improve the physical robustness of such supramolecular systems.

CRediT authorship contribution statement

Zhenping Shi: Writing – original draft, Validation, Investigation, Formal analysis. **Matthew Hyder:** Writing – original draft, Visualization, Validation, Investigation, Formal analysis, Conceptualization. **Alarqam Z. Tareq:** Writing – original draft, Validation, Investigation, Formal analysis. **Ann M. Chippindale:** Writing – review & editing, Formal analysis. **James A. Cooper:** Writing – review & editing, Supervision. **Josephine L. Harries:** Writing – review & editing, Supervision. **Wayne Hayes:** Writing – review & editing, Supervision, Resources, Project administration, Conceptualization.

Declaration of competing interest

The authors declare that they have no known competing financial interests or personal relationships that could have appeared to influence the work reported in this paper.

Data availability

Data will be made available on request.

Acknowledgements

The authors would like to acknowledge the financial support from the University of Reading and Domino Printing Sciences Ltd. (PhD studentship for M.H.) and from HCED Iraq (PhD studentship for A.Z.T.). In addition, the University of Reading (EPSRC – Doctoral Training Grant) is acknowledged for providing access to instrumentation in the Chemical Analysis Facility and the Centre for Advanced Microscopy. We thank Mr. Nick Spencer (Chemical Analysis Facility (CAF), University of Reading) for collecting the single-crystal X-ray data.

Appendix A. Supplementary data

Supplementary data to this article can be found online at https://doi.org/10.1016/j.reactfunctpolym.2024.105994.

References

[1] A.D. O'Donnell, S. Salimi, L.R. Hart, T.S. Babra, B.W. Greenland, W. Hayes, Applications of supramolecular polymer networks, React. Funct. Polym. 172 (2022) 105209, https://doi.org/10.1016/j.reactfunctpolym.2022.105209.
[2] L.R. Hart, J.L. Harries, B.W. Greenland, H.M. Colquhoun, W. Hayes, Healable supramolecular polymers, Polym. Chem. 4 (2013) 4860–4870, https://doi.org/10.1039/c3py00081h.
[3] X. Chen, C.E. Zawaski, G.A. Spiering, B. Liu, C.M. Orsino, R.B. Moore, C. B. Williams, T.E. Long, Quadruple hydrogen bonding supramolecular elastomers for melt extrusion additive manufacturing, ACS Appl. Mater. Interfaces 12 (2020) 32006–32016, https://doi.org/10.1021/acsami.0c08958.
[4] Y. Yanagisawa, Y. Nan, K. Okuro, T. Aida, Mechanically robust, readily repairable polymers via tailored noncovalent cross-linking, Science 359 (2018) (1979) 72–76, https://doi.org/10.1126/science.aam7588.
[5] P.J. Woodward, D. Hermida Merino, B.W. Greenland, I.W. Hamley, Z. Light, A. T. Slark, W. Hayes, Hydrogen bonded supramolecular elastomers: correlating hydrogen bonding strength with morphology and rheology, Macromolecules 43 (2010) 2512–2517, https://doi.org/10.1021/ma9027646.
[6] J.B. Beck, J.M. Ineman, S.J. Rowan, Metal/ligand-induced formation of Metallo-supramolecular polymers, Macromolecules 38 (2005) 5060–5068, https://doi.org/10.1021/ma050369e.
[7] C. Heinzmann, S. Coulibaly, A. Roulin, G.L. Fiore, C. Weder, Light-induced bonding and Debonding with supramolecular adhesives, ACS Appl. Mater. Interfaces 6 (2014) 4713–4719, https://doi.org/10.1021/AM405302Z.
[8] S. Chen, Z. Li, Y. Wu, N. Mahmood, F. Lortie, J. Bernard, W.H. Binder, J. Zhu, Hydrogen-bonded supramolecular polymer adhesives: straightforward synthesis and strong substrate interaction, Angew. Chem. Int. Ed. 61 (2022) e202203876, https://doi.org/10.1002/anie.202203876.
[9] S. Chen, Z. Geng, X. Zheng, J. Xu, W.H. Binder, J. Zhu, Engineering the morphology of hydrogen-bonded comb-shaped supramolecular polymers: from solution self-assembly to confined assembly, Polym. Chem. 11 (2020) 4022–4028, https://doi.org/10.1039/D0PY00570C.
[10] M. Nakahata, Y. Takashima, A. Harada, Highly Flexible, Tough, and Self-Healing Supramolecular Polymeric Materials Using Host–Guest Interaction, Macromol. Rapid Commun. 37 (2016) 86–92, https://doi.org/10.1002/marc.201500473.
[11] K. Yamauchi, J.R. Lizotte, T.E. Long, Thermoreversible poly(alkyl acrylates) consisting of self-complementary multiple hydrogen bonding, Macromolecules 36 (2003) 1083–1088, https://doi.org/10.1021/ma0212801.
[12] R.P. Sijbesma, F.H. Beijer, L. Brunsveld, B.J.B. Folmer, J.H.K.K. Hirschberg, R.F. M. Lange, J.K.L. Lowe, E.W. Meijer, Reversible polymers formed from self-

complementary monomers using quadruple hydrogen bonding, Science 278 (1997) (1979) 1601–1604, https://doi.org/10.1126/science.278.5343.1601.
[13] B.J.B. Folmer, R.P. Sijbesma, R.M. Versteegen, J.A.J. van der Rijt, E.W. Meijer, Supramolecular polymer materials:chain extension of telechelic polymers usinga reactive hydrogen-bonding synthon, Adv. Mater. 12 (2000) 874–878, https://doi.org/10.1002/1521-4095(200006)12:12<874::AID-ADMA874>3.0.CO;2-C.
[14] A. Feula, A. Pethybridge, I. Giannakopoulos, X. Tang, A. Chippindale, C.R. Siviour, C.P. Buckley, I.W. Hamley, W. Hayes, A Thermoreversible supramolecular polyurethane with excellent healing ability at 45 °c, Macromolecules 48 (2015) 6132–6141, https://doi.org/10.1021/acs.macromol.5b01162.
[15] A. Feula, X. Tang, I. Giannakopoulos, A.M. Chippindale, I.W. Hamley, F. Greco, C. P. Buckley, C.R. Siviour, W. Hayes, An adhesive elastomeric supramolecular polyurethane healable at body temperature, Chem. Sci. 7 (2016) 4291–4300, https://doi.org/10.1039/C5SC04864H.
[16] M. Hyder, A.D. O'Donnell, A.M. Chippindale, I.M. German, J.L. Harries, O. Shebanova, I.W. Hamley, W. Hayes, Tailoring viscoelastic properties of dynamic supramolecular poly(butadiene)-based elastomers, Mater. Today Chem. 26 (2022) 101008, https://doi.org/10.1016/J.MTCHEM.2022.101008.
[17] S. Burattini, H.M. Colquhoun, J.D. Fox, D. Friedmann, B.W. Greenland, P.J. F. Harris, W. Hayes, M.E. Mackay, S.J. Rowan, A self-repairing, supramolecular polymer system: healability as a consequence of donor–acceptor π–π stacking interactions, Chem. Commun. (2009) 6717–6719, https://doi.org/10.1039/b910648k.
[18] S. Burattini, B.W. Greenland, D.H. Merino, W. Weng, J. Seppala, H.M. Colquhoun, W. Hayes, M.E. Mackay, I.W. Hamley, S.J. Rowan, A healable supramolecular polymer blend based on aromatic π−π stacking and hydrogen-bonding interactions, J. Am. Chem. Soc. 132 (2010) 12051–12058, https://doi.org/10.1021/ja104446r.
[19] J. Fox, J.J. Wie, B.W. Greenland, S. Burattini, W. Hayes, H.M. Colquhoun, M. E. Mackay, S.J. Rowan, High-strength, healable, supramolecular polymer nanocomposites, J. Am. Chem. Soc. 134 (2012) 5362–5368, https://doi.org/10.1021/ja300050x.
[20] D. Knapton, S.J. Rowan, C. Weder, Synthesis and properties of Metallo-supramolecular poly(p-phenylene ethynylene)s, Macromolecules 39 (2006) 651–657, https://doi.org/10.1021/ma0520747.
[21] D. Knapton, P.K. Iyer, S.J. Rowan, C. Weder, Synthesis and properties of Metallo-supramolecular poly(p-xylylene)s, Macromolecules 39 (2006) 4069–4075, https://doi.org/10.1021/ma060500y.
[22] S. Dong, B. Zheng, F. Wang, F. Huang, Supramolecular Polymers Constructed from Macrocycle-Based Host–Guest Molecular Recognition Motifs, Acc. Chem. Res. 47 (2014) 1982–1994, https://doi.org/10.1021/ar5000456.
[23] D. Xia, P. Wang, X. Ji, N.M. Khashab, J.L. Sessler, F. Huang, Functional supramolecular polymeric networks: the marriage of covalent polymers and macrocycle-based host–guest interactions, Chem. Rev. 120 (2020) 6070–6123, https://doi.org/10.1021/acs.chemrev.9b00839.
[24] M. Chen, D.L. Inglefield, K. Zhang, A.G. Hudson, S.J. Talley, R.B. Moore, T.E. Long, Synthesis of urea-containing ABA triblock copolymers: influence of pendant hydrogen bonding on morphology and thermomechanical properties, J. Polym. Sci., Part A: Polym. Chem. 56 (2018) 1844–1852, https://doi.org/10.1002/pola.29066.
[25] B.D. Mather, M.B. Baker, F.L. Beyer, M.A.G. Berg, M.D. Green, T.E. Long, Supramolecular triblock copolymers containing complementary nucleobase molecular recognition, Macromolecules 40 (2007) 6834–6845, https://doi.org/10.1021/ma070865y.
[26] S. Cheng, M. Zhang, N. Dixit, R.B. Moore, T.E. Long, Nucleobase self-assembly in supramolecular adhesives, Macromolecules 45 (2012) 805–812, https://doi.org/10.1021/ma202122r.
[27] K. Zhang, M. Aiba, G.B. Fahs, A.G. Hudson, W.D. Chiang, R.B. Moore, M. Ueda, T. E. Long, Nucleobase-functionalized acrylic ABA triblock copolymers and supramolecular blends, Polym. Chem. 6 (2015) 2434–2444, https://doi.org/10.1039/C4PY01798F.
[28] C.L. Elkins, T. Park, M.G. McKee, T.E. Long, Synthesis and characterization of poly (2-ethylhexyl methacrylate) copolymers containing pendant, self-complementary multiple-hydrogen-bonding sites, J. Polym. Sci., Part A: Polym. Chem. 43 (2005) 4618–4631, https://doi.org/10.1002/pola.20961.
[29] D.W.R. Balkenende, C.A. Monnier, G.L. Fiore, C. Weder, Optically responsive supramolecular polymer glasses, Nat. Commun. 7 (2016) 10995, https://doi.org/10.1038/ncomms10995.
[30] Y. Chen, A.M. Kushner, G.A. Williams, Z. Guan, Multiphase design of autonomic self-healing thermoplastic elastomers, Nat. Chem. 4 (2012) 467–472, https://doi.org/10.1038/nchem.1314.
[31] C. Kim, K.T. Kim, Y. Chang, H.H. Song, T.-Y. Cho, H.-J. Jeon, Supramolecular assembly of amide Dendrons, J. Am. Chem. Soc. 123 (2001) 5586–5587, https://doi.org/10.1021/ja015687h.
[32] N.S. Murthy, Hydrogen bonding, mobility, and structural transitions in aliphatic polyamides, J. Polym. Sci. B Polym. Phys. 44 (2006) 1763–1782, https://doi.org/10.1002/polb.20833.
[33] K. Marchildon, Polyamides – still strong after seventy years, Macromol. React. Eng. 5 (2011) 22–54, https://doi.org/10.1002/mren.201000017.
[34] P.J.M. Stals, M.M.J. Smulders, R. Martín-Rapún, A.R.A. Palmans, E.W. Meijer, Asymmetrically Substituted Benzene-1,3,5-tricarboxamides: Self-Assembly and Odd–Even Effects in the Solid State and in Dilute Solution, Chem. Eur. J. 15 (2009) 2071–2080, https://doi.org/10.1002/chem.200802196.
[35] S. Cantekin, T.F.A. de Greef, A.R.A. Palmans, Benzene-1,3,5-tricarboxamide: a versatile ordering moiety for supramolecular chemistry, Chem. Soc. Rev. 41 (2012) 6125–6137, https://doi.org/10.1039/c2cs35156k.
[36] K.E. Broaders, S.J. Pastine, S. Grandhe, J.M.J. Fréchet, Acid-degradable solid-walled microcapsules for pH-responsive burst-release drug delivery, Chem. Commun. 47 (2011) 665–667, https://doi.org/10.1039/C0CC04190D.
[37] M. de Loos, J.H. van Esch, R.M. Kellogg, B.L. Feringa, C3-symmetric, amino acid based organogelators and thickeners: a systematic study of structure–property relations, Tetrahedron 63 (2007) 7285–7301, https://doi.org/10.1016/j.tet.2007.02.066.
[38] C.F.C. Fitié, W.S.C. Roelofs, M. Kemerink, R.P. Sijbesma, Remnant polarization in thin films from a columnar liquid crystal, J. Am. Chem. Soc. 132 (2010) 6892–6893, https://doi.org/10.1021/ja101734g.
[39] C.F.C. Fitié, I. Tomatsu, D. Byelov, W.H. de Jeu, R.P. Sijbesma, Nanostructured materials through orthogonal self-assembly in a columnar liquid crystal, Chem. Mater. 20 (2008) 2394–2404, https://doi.org/10.1021/cm703508t.
[40] J. Roosma, T. Mes, P. Leclère, A.R.A. Palmans, E.W. Meijer, Supramolecular materials from Benzene-1,3,5-tricarboxamide-based Nanorods, J. Am. Chem. Soc. 130 (2008) 1120–1121, https://doi.org/10.1021/ja0774764.
[41] A.Z. Tareq, M. Hyder, D.H. Merino, A.M. Chippindale, A. Kaur, J.A. Cooper, W. Hayes, Thermally and mechanically robust self-healing supramolecular polyurethanes featuring aliphatic amide end caps, Polymer (Guildf) (2024) 127052, https://doi.org/10.1016/j.polymer.2024.127052.
[42] D. Kim, S. Lee, Y. Choi, S. Hwang, S. Kuo, C. Nah, M. Lee, K. Jeong, Thermal- and photo-induced phase-transition behaviors of a tapered dendritic liquid crystal with photochromic Azobenzene Mesogens and a bicyclic chiral center, Chem. Eur. J. 20 (2014) 5689–5695, https://doi.org/10.1002/chem.201303924.
[43] E. Wuckert, M.D. Harjung, N. Kapernaum, C. Mueller, W. Frey, A. Baro, F. Giesselmann, S. Laschat, Photoresponsive ionic liquid crystals based on azobenzene guanidinium salts, Phys. Chem. Chem. Phys. 17 (2015) 8382–8392, https://doi.org/10.1039/C4CP04783D.
[44] F. Mu, S.L. Coffing, D.J. Riese, R.L. Geahlen, P. Verdier-Pinard, E. Hamel, J. Johnson, M. Cushman, Design, synthesis, and biological evaluation of a series of Lavendustin a analogues that inhibit EGFR and Syk tyrosine kinases, as well as tubulin polymerization, J. Med. Chem. 44 (2001) 441–452, https://doi.org/10.1021/jm000387g.
[45] D. Nicholls, C. Elleman, N. Shankland, K. Shankland, A new crystalline form of αβ-D-lactose prepared by oven drying a concentrated aqueous solution of D-lactose, Acta Crystallogr. Sect. C Struct. Chem. 75 (2019) 904–909, https://doi.org/10.1107/S2053229619008210.
[46] L. Palatinus, G. Chapuis, SUPERFLIP – a computer program for the solution of crystal structures by charge flipping in arbitrary dimensions, J. Appl. Crystallogr. 40 (2007) 786–790, https://doi.org/10.1107/S0021889807029238.
[47] P.W. Betteridge, J.R. Carruthers, R.I. Cooper, K. Prout, D.J. Watkin, CRYSTALS version 12: software for guided crystal structure analysis, J. Appl. Crystallogr. 36 (2003) 1487, https://doi.org/10.1107/S0021889803021800.
[48] S. Rogers, L. Mandelkern, Glass transitions of the poly-(n-alkyl Methacrylates), J. Phys. Chem. 61 (1957) 985–991, https://doi.org/10.1021/j150553a033.
[49] J. Lal, G.S. Trick, Glass transformation temperatures of poly(vinyl alkyl ethers) and poly(vinyl alkyl sulfides), J. Polym. Sci., Part A: Gen. Pap. 2 (1964) 4559–4572, https://doi.org/10.1002/pol.1964.100021024.
[50] H.A. Schneider, Polymer class specificity of the glass temperature, Polymer (Guildf) 46 (2005) 2230–2237, https://doi.org/10.1016/j.polymer.2004.07.054.
[51] M.C. Stuparu, A. Khan, C.J. Hawker, Phase separation of supramolecular and dynamic block copolymers, Polym. Chem. 3 (2012) 3033–3044, https://doi.org/10.1039/c2py20368e.
[52] L.T.J. Korley, B.D. Pate, E.L. Thomas, P.T. Hammond, Effect of the degree of soft and hard segment ordering on the morphology and mechanical behavior of semicrystalline segmented polyurethanes, Polymer (Guildf) 47 (2006) 3073–3082, https://doi.org/10.1016/j.polymer.2006.02.093.
[53] T. Jing, X. Heng, X. Guifeng, L. Li, P. Li, X. Guo, Rapid self-healing and tough polyurethane based on the synergy of multi-level hydrogen and disulfide bonds for healing propellant microcracks, Mater. Chem. Front. 6 (2022) 1161–1171, https://doi.org/10.1039/D2QM00047D.
[54] J. He, F. Song, X. Li, L. Chen, X. Gong, W. Tu, A novel kind of room temperature self-healing poly(urethane-urea) with robust mechanical strength based on aromatic disulfide, J. Polym. Res. 28 (2021) 122, https://doi.org/10.1007/s10965-021-02433-0.
[55] J.J.B. van der Tol, G. Vantomme, A.R.A. Palmans, E.W. Meijer, Controlling the Processability and stability of supramolecular polymers using the interplay of intra- and intermolecular interactions, Macromolecules 55 (2022) 6820–6829, https://doi.org/10.1021/acs.macromol.2c00976.
[56] Y. Wu, L. Wang, X. Zhao, S. Hou, B. Guo, P.X. Ma, Self-healing supramolecular bioelastomers with shape memory property as a multifunctional platform for biomedical applications via modular assembly, Biomater 104 (2016) 18–31, https://doi.org/10.1016/j.biomaterials.2016.07.011.
[57] S. Salimi, Y. Wu, M.I.E. Barreiros, A.A. Natfji, S. Khaled, R. Wildman, L.R. Hart, F. Greco, E.A. Clark, C.J. Roberts, W. Hayes, A 3D printed drug delivery implant formed from a dynamic supramolecular polyurethane formulation, Polym. Chem. 11 (2020) 3453–3464, https://doi.org/10.1039/D0PY00068J.
[58] B.C. Baker, I.M. German, G.C. Stevens, H.M. Colquhoun, W. Hayes, Synthesis and analysis of a healable, poly(propylene glycol)-based supramolecular network, Prog. Org. Coat. 127 (2019) 260–265, https://doi.org/10.1016/j.porgcoat.2018.11.029.
[59] Y. Chen, Z. Guan, Multivalent hydrogen bonding block copolymers self-assemble into strong and tough self-healing materials, Chem. Commun. 50 (2014) 10868–10870, https://doi.org/10.1039/C4CC03168G.
[60] J. Hentschel, A.M. Kushner, J. Ziller, Z. Guan, Self-healing supramolecular block copolymers, Angew. Chem. Int. Ed. 51 (2012) 10561–10565, https://doi.org/10.1002/anie.201204840.

[61] Y. Chen, Z. Guan, Self-healing thermoplastic elastomer brush copolymers having a glassy polymethylmethacrylate backbone and rubbery polyacrylate-amide brushes, Polymer (Guildf) 69 (2015) 249–254, https://doi.org/10.1016/j.polymer.2015.03.023.
[62] A. del Prado, D.K. Hohl, S. Balog, L.M. de Espinosa, C. Weder, Plant oil-based supramolecular polymer networks and composites for Debonding-on-demand adhesives, ACS Appl. Polym. Mater. 1 (2019) 1399–1409, https://doi.org/10.1021/acsapm.9b00175.
[63] Q. Zhang, C.Y. Shi, D.H. Qu, Y.T. Long, B.L. Feringa, H. Tian, Exploring a naturally tailored small molecule for stretchable, self-healing, and adhesive supramolecular polymers, Sci. Adv. 4 (2018) eaat8192, https://doi.org/10.1126/sciadv.aat8192.
[64] D. Wang, J. Xu, J. Chen, P. Hu, Y. Wang, W. Jiang, J. Fu, Transparent, mechanically strong, extremely tough, self-recoverable, healable supramolecular elastomers facilely fabricated via dynamic hard domains Design for Multifunctional Applications, Adv. Funct. Mater. 30 (2020) 1907109, https://doi.org/10.1002/adfm.201907109.